Fast–ICA for Mechanical Fault Detection and Identification in Electromechanical Systems for Wind Turbine Applications

Mohamed Farhat
Department of Electrical Engineering, University of Tunis El Manar, LA.R.A. Automatique, National Engineering School of Tunis, BP 37, 1002 Tunis, Tunisia

Yasser Gritli
Department of Electrical Engineering, University of Tunis El Manar, LA.R.A. Automatique, National Engineering School of Tunis, BP 37, 1002 Tunis, Tunisia

Mohamed Benrejeb
Department of Electrical Engineering, University of Tunis El Manar, LA.R.A. Automatique, National Engineering School of Tunis, BP 37, 1002 Tunis,Tunisia

***Abstract*—Recently, the approaches based on source separation are increasingly adopted for the fault diagnosis in several industrial applications. In particular, Independent Component Analysis (ICA) method is attractive, thanks to its simplicity of implementation. In the context of electrical rotating machinery with a variable speed, namely the wind turbine type, the interaction between the electrical and mechanical parts along with the fault is complex. Therefore, the essential system variables are affected and it thereby requires to be analyzed in order to detect the presence of certain faults. In this paper, the target system is the classical association of a doubly-fed induction motor to a two stage gearbox for wind energy application system. The investigated mechanical fault is a uniform wear of two gear wheels for the same stage. The idea behind the proposed technique is to consider the fault detection and identification as a source separation problem. Based on the analysis into independent components, Fast–ICA algorithm is adopted to separate and identify the sources of the gear faults. Afterwards, a spectral analysis is applied on the signals resulting from the separation in order to identify the fault components related to the damaged wheels. The efficiency of the proposed technique for the separation and identification of the fault components is evaluated by numerical simulations.**

***Keywords*—Source separation; fault diagnosis; independent component analysis; fast–ICA; spectral analysis**

I. INTRODUCTION

Wind power increasingly gain ground, thanks to its characteristics as an inexhaustible and clean source of energy, which has made it a privileged field of scientific research and technological development in the world. A recent report shows the large-scale expansion of the installation of wind farms in the world [1]. Yet, an electric machine, whether running as a motor or as a generator, is rather sized in torque.

In small powers, the speed is relatively high, however in the case of large powers, (several hundred KW to a few MW), the low speeds lead to very high torques and prohibitive generator masses. For this reason, a gearbox is typically interposed between the turbine and the generator. Consequently, the fast shaft of the gearbox is coupled to the shaft of the electric generator [2], [3], [4]. A recent study of faults in the wind energy conversion systems revealed that about 10% of the identified defects are related to the gearbox [5], [6]. Although this proportion is apparently low, this type of fault often leads to prohibitive production stops. That's from where comes the need to continuously monitor the proper functioning of this essential component in the energy conversion chain. That is why, several diagnostic techniques for the fault detection in these speed multipliers have been developed. These techniques include: Analysis of acoustic emissions [7], [8], oil analysis [9], [11] and specifically vibratory analysis. In particular, the investigation of vibratory signals has been proposed in different works, using different approaches: statistical analysis [10]-[11], temporal and/or frequency domain [7], [12], [13].

In reality, the vibratory signals collected during operation contain relevant informations which reflect several sources of faults relating to the speed multiplier itself and to those associated with the machine coupled with it. This is clearly justified in the references [14], [15], where the characterization of bar breaking faults, as well as the unbalance was based on the time-frequency analysis of the vibratory signals.

However, the measured observations are often mixtures of the vibrations of the defects mentioned before. This makes the diagnosis of defects a very difficult task. To solve this problem, several techniques have been used to identify the sources of defects from the spectral mixtures resulting from vibratory signals [16], [17], [18].

In the literature, Independent Component Analysis (ICA) has been widely applied for the separation of sources in different domains, including medical imagery, telecommunications, and more recently for the diagnosis of faults in electromechanical systems [19], [20], [21], [22].

More recently, new ICA-based techniques have been proposed for fault diagnosis in the electromechanical systems. In fact, the most used algorithms of the (ICA) can be classified as follows

- The InfoMax algorithm [23] solves the ICA problem by maximizing the differential entropy of the output of an invertible non-linear transformation of the whitened observations;

- JADE [24]-[25] consists in jointly diagonalizing the set of the eigen-matrices constructed from the eigenvectors associated to the *P* greatest eigenvalues of the covariance matrix of the whitened observations;
- Fast–ICA [26] tries, after the whitening step, to maximize a contrast function based on negentropy.

In the present work, the fast temporal algorithm, known as Fast–ICA , has been adopted for the identification of gear faults because of its appealing characteristics: high convergence speed and low computational cost. Moreover, this technique is interesting since it is relatively insensitive to the increase in the number of sources. This paper is organized as follows: Fast-ICA is formulated for fault diagnosis in the second section. Then, the gear vibration data is described in the third section. Afterwards, the fourth section is dedicated for the spectral analysis. Finally, the paper ends with a conclusion.

II. Formulation of The Fast–ICA for Fault Diagnosis

The Fast–ICA algorithm is an advanced version of the ICA, characterized mainly by a very fast convergence, whose separation into independent components takes place in a whitened space [27],[28]. In fact, instantaneous linear mixtures (signals from sensors) are preprocessed. This consists in their projection into a whitened space. Then, they are separated by the Fast–ICA algorithm itself. The details of these two preprocessing steps and the Fast–ICA processing are described in the following. Furthermore, several nonlinearity functions are presented because of their impact on the performance of Fast–ICA algorithm.

A. Preprocessing step

Let *n* sources of faults s_j denoted by $[s_1, ..., s_n]^T$, and mixed before being retrieved by the sensors. Thus, *m* mixtures x_i of length *N*, are represented as rows of a *m*x*N* matrix denoted $X = [x_1, ..., x_m]^T$.

$$X = \begin{pmatrix} X_{1,1} & \cdots & \cdots & \cdots & X_{1,N} \\ \vdots & \cdots & X_{i,j} & \cdots & \vdots \\ X_{m,1} & \cdots & \cdots & \cdots & X_{m,N} \end{pmatrix} \quad (1)$$

Moreover, it can be represented by a linear model as

$$X = AS + bh \quad (2)$$

where *A* is an $m \times n$ mixing matrix, *h* is the additive noise with the corresponding Gaussian weight vector given by $b = [b_1,..., b_n]^T$.

In order to apply Principal Component Analysis (PCA) to the mixtures, they should be considered differently. Indeed, the mixtures *X* should be seen as a set of *N* m-dimensional points. Now, each column of *X* is interpreted as the coordinates of a point in the space $\mathbb{R}^m$.

First of all, PCA computes the mean of the *N* points, denoted $\mu = (\mu_1, ... \mu_m)^T$, as follows

$$\mu_i = \frac{1}{N}\sum_{j=1}^{N} X_{i,j}, \text{ for all } i=1,\ldots,m \quad (3)$$

Then, PCA centers each point relatively to μ as follows:

$$(X'_{1,j}, ... X'_{m,j})^T = (X_{1,j}, ... X_{m,j})^T - (\mu_1, ... \mu_m)^T, \text{ for all } j=1,\ldots, N \quad (4)$$

Therefore, the resulting matrix denoted *X'* has as rows the centered mixtures.

$$X' = \begin{pmatrix} X'_{1,1} & \cdots & X'_{1,j} & \cdots & X'_{1,N} \\ \vdots & \cdots & \vdots & \cdots & \vdots \\ X'_{m,1} & \cdots & X'_{m,j} & \cdots & X'_{m,N} \end{pmatrix} \quad (5)$$

Afterwards, the covariance matrix $\mathcal{C}$ of *X'* is computed as follows

$$\mathcal{C} = \frac{1}{N-1} X'X'^T \quad (6)$$

Then, the $\mathcal{C}$ matrix is diagonalized as follows

$$\mathcal{C} = EDE^T \quad (7)$$

Therefore, two matrices are obtained

- a diagonal matrix denoted *D* composed of decreasingly sorted eigenvalues of the covariance matrix of *X'*.
- a matrix denoted *E* whose columns are the eigenvectors of the covariance matrix of *X'*. These eigenvectors are pairwise orthogonal.

Once PCA achieved, the whitening matrix denoted *U* is calculated by the following expression

$$U = D^{-\frac{1}{2}}E^T \quad (8)$$

Finally, this steps results in the matrix composed of whitened mixtures, denoted *V*, is obtained by

$$V = UX \quad (9)$$

B. Processing Step: Implementation of the "Fast–ICA " fixed point algorithm

The ICA method defines a separation model in order to estimate the sources $\hat{S}$ given the whitened mixtures *V*

$$\hat{S} = W^T V \quad (10)$$

Therefore, the goal of the ICA subsequently is to estimate W^T, called the whitened separation matrix.In particular, the Fast–ICA estimates the independent components by maximizing the non-gaussianity, defined as the opposite of the deviation of this signal distribution relatively to a gaussian signal distribution of the same power. It is thus possible to separate the sources of a linear mixture by maximizing the non-gaussianity of the obtained output signal by a linear combination of the observations.

There are multiple approaches to measure the non-gaussianity. After several trials with different approaches, mainly: normalized kurtosis, negentropy, [26], [29], the authors in the literature opted for negentropy. Next, the steps of the Fast–ICA algorithm are described, represented by the flowchart of Figure 1.

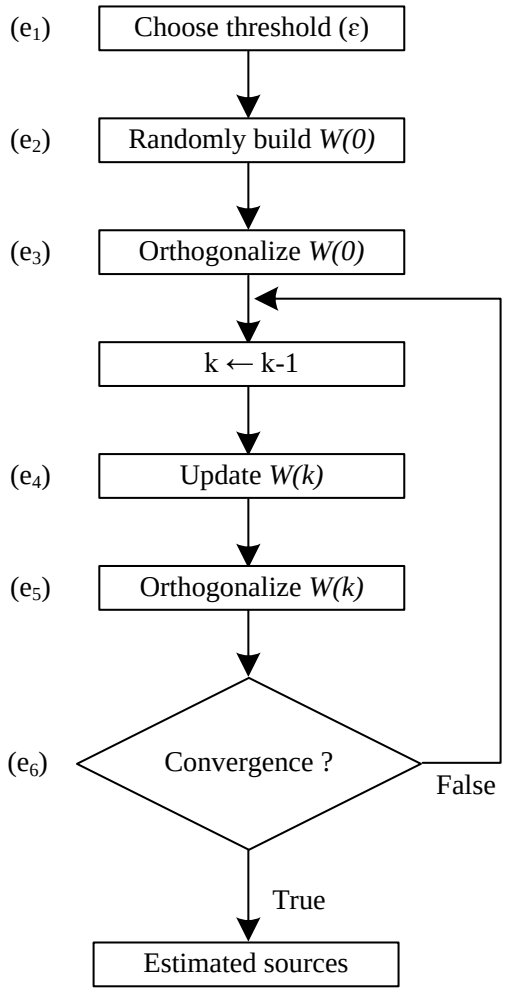

Fig. 1. Flowchart of FastICA.

Indeed, the application of the Fast–ICA algorithm starts with

step (e_1) which assigns a positive and infinitely small value to a parameter, called convergence threshold and denoted ε.

The next initialization step denoted (e_2) consists in constructing *W(k)*, as well as its zero-order orthogonalization in step (e_3). Thereafter, the algorithm iteratively performs the following two steps

- step (e_4) of updating the matrix *W* to the order *k* is performed by the following equation of the fixed point of the negentropy

$$W(k) = E\{Vg(W^T(k-1)V)\} - E\{Vg'(W^T(k-1)V)\} \quad (11)$$

where the function *g* is representing the non-linearity of the Fast–ICA algorithm, which will be detailed later.

- the orthogonalization step (e_5) based on the symmetric method, which does not favor any vector *w*, consists of starting directly from any matrix *W*, orthogonalizing it by the Gram-Schmidt approach, as follows

$$W(k) \leftarrow \left(W(k)W^T(k)\right)^T W(k) \quad (12)$$

- finally, at the end of each iteration, the algorithm checks in step (e_6) whether it has reached a maximum of the negentropy, which is based on the thresholding process given by

$$1 - \|W^T(k)W(k-1)\| < \varepsilon \quad (13)$$

C. Choice of the nonlinearity:

The function g of equation (11) is the non-linearity of Fast–ICA, which can be, as shown in the literature

- tangent-hyperbolic noted g_1 which is effective for any type of situation

$$g_1 = tanh(y) \quad (14)$$

- kurtosis noted g_2 which is used only in the case of subgaussian variables

$$g_2 = y^3 \quad (15)$$

- exponential or Gauss noted g_3 which is more suitable in the case of supergaussian variables

$$g_3 = ye^{-\frac{y^2}{2}} \quad (16)$$

- skewness noted g_4 is the third level moment which measures the asymmetry of the data

$$g_4 = \frac{y^2}{2} \quad (17)$$

The choice of the function g has a direct impact on the updating of *W* as indicated in equation (12), and consequently on the overall performance of the algorithm.

III. Presentation of Gear Vibration Data

A. System Description

In order to evaluate the efficiency of the method described above, the asynchronous double-feed machine-speed multiplier combination of Figure 2 has been considered.

More precisely, the defects relating to the gear- A two-stage speed multiplier are interesting. Indeed, the gear in question is composed of four toothed wheels (R1, R2, R3 and R4). The system under consideration is assumed to operate at nominal speed of 1012 rpm on the side of the generator (Wheel R4) and 46 rpm on the turbine side (Wheel R1).

In fact, the vibrations resulting from the gearbox operation are due to the forces of mutual contact between the teeth of the wheels in contact. For two wheels, of the same stage, making contact, a meshing frequency is given by

$$f_{mesh} = f_{r,i}Z_i = f_{r,i+1}Z_{i+1} \quad (18)$$

where the $f_{r,i}$ and $f_{r,i+1}$ are the rotational frequencies of the wheels for the same considered stage. The numbers of teeth relative to each wheel are denoted Z_i and Z_{i+1}.

Under healthy gear, the vibration spectrum typically shows the harmonic chain in (19) with small amplitudes.

$$f_{sideband} = kf_{mesh} \pm f_{r,i} \quad (19)$$

On the other hand, in presence of a uniform wear fault on all the teeth of the same wheel, the amplitude of the harmonics in (19) shows a noticeable increase, making it possible to

identify the wheel affected by the fault. In the considered system, the wheels R1 and R2 have the same meshing frequency $f_{mesh1,2}$ and have respectively different lateral frequencies (f_{l1},f_{r1}) and (f_{l2},f_{r2}).

Likewise, the wheels R3 and R4 have the same meshing frequency $f_{eng3,4}$ and have respectively different lateral frequencies (f_{g3},f_{d3}) and (f_{g4},f_{d4}), as detailed in Table I.

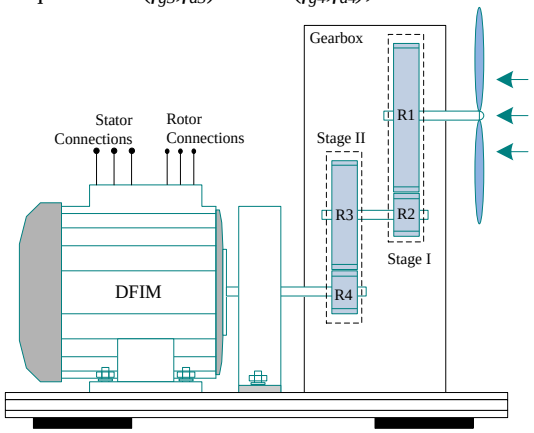

Fig. 2. Simplified representation of the generator association with double-fed multiplier of speed composed of two stages.

TABLE I. FREQUENCIES OF FAULT IDENTIFICATION

	Rotating Speed (tr/min)	**Number of teeth Z_i**	$f_{lk,\ (k=1..4)}$	$f_{rk,\ (k=1..4)}$
R1	46	69	52.12	53.66
R2	186.7	17	49.78	56
R3	186.7	92	283.62	289.84
R4	1012	17	269.87	303.59

B. *Description of mixtures*

The mixtures are linear combinations of the sources as indicated in equation (2), where matrix *A* and vector *b* must be specified

- the adopted mixture matrix *A* is chosen as

$$A = \begin{pmatrix} 0.9 & 053 & 0.7 & 0.6 \\ 0.45 & 0.9 & 0.68 & 0.55 \\ 0.55 & 0.71 & 0.9 & 0.6 \\ 0.6 & 0.52 & 0.7 & 0.9 \end{pmatrix} \quad (20)$$

- the vector *b*, of dimension 4×1, for the weighting of noise in the mixtures

$$b = \begin{pmatrix} 0.3 \\ 0.5 \\ 0.7 \\ 0.1 \end{pmatrix} \quad (21)$$

On the other hand, a mixture can be represented either in the temporal space or in the spectral space. Nevertheless, the choice of the appropriate representation is required. It allows to know whether a mixture is in healthy mode or in faulty mode.

The temporal representation of the mixtures makes it possible to distinguish the healthy mode from the faulty mode. Indeed, the amplitudes in the faulty mode shown in Figure 4 are generally greater than the amplitudes in the healthy mode illustrated in Figure 3. However, the problem is that the temporal representation does not make possible to display exactly which wheels are affected by the fault. For this purpose, it is preferred to use the spectral representation instead of the temporal representation.

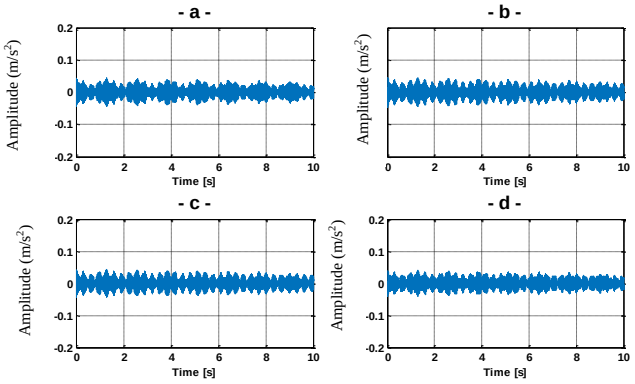

Fig. 3. Mixtures used for the separation under healthy condition.

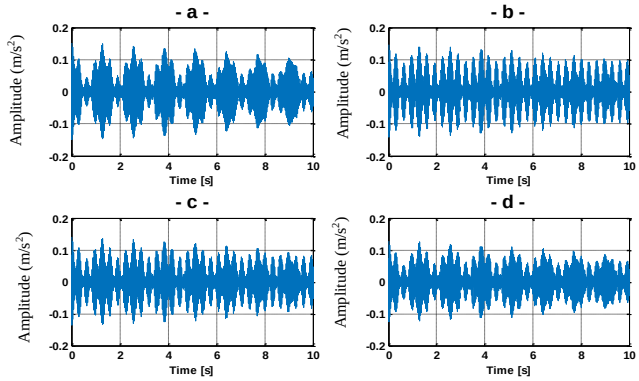

Fig. 4. Mixtures used for the separation under a uniform wear of R1 and R2.

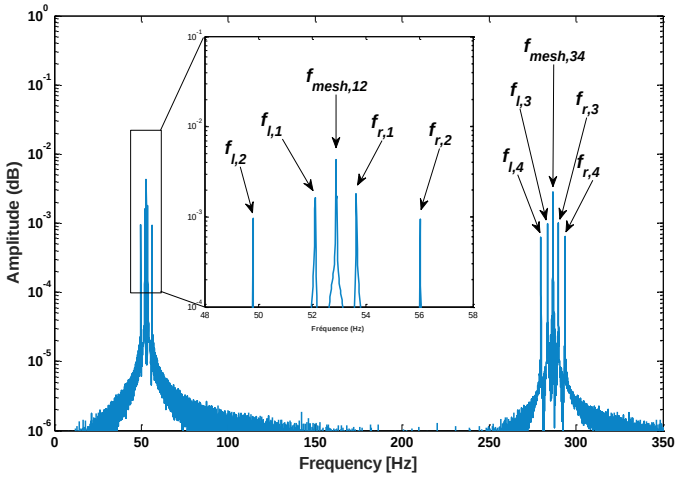

Fig. 5. Spectrum of mixture 1, in healthy mode.

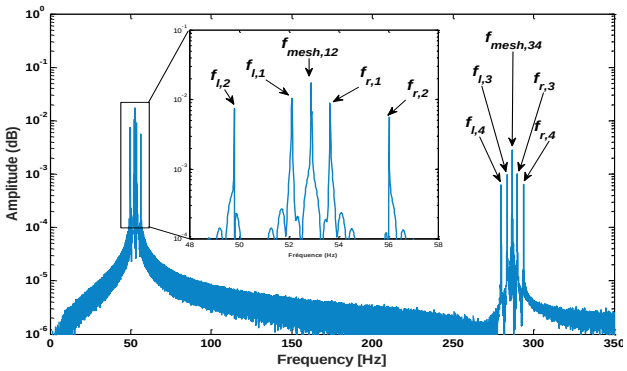

Fig. 6. Spectrum of mixture 1, under a uniform wear of R1 and R2.

For instance, for the frequency-band centered at f_{mesh34}, the spectrum of mixture 1 in the faulty mode, presented in Figure 6, is similar to the spectrum of this mixture in the healthy mode, in Figure 5. This result shows that the wheels R3 and R4 are healthy.

On the other hand, for the frequency-band centered in f_{mesh12}, the spectrum of mixture 1 in the fault mode, in Figure 6, is different from the spectrum of the same mixture in the healthy mode, in Figure 5. This proves that the wheels R1 and R2 are affected by the uniform wear fault.

C. Study of the whitening preprocessing

The mixtures are firstly whitened using Principal Component Analysis (PCA) technique.

Let x be the sample composed of points in $\mathbb{R}^4$ extracted from the mixtures X in the faulty mode, Figure 7. PCA computes the two following moments of x

- the arithmetic mean

$$\mu = (0\ 0\ 0\ 0)^T \tag{22}$$

- the covariance matrix

$$\mathcal{C} = 10^{-4}\begin{pmatrix} 17 & 18 & 15 & 13 \\ 18 & 21 & 17 & 14 \\ 15 & 17 & 14 & 12 \\ 13 & 14 & 12 & 10 \end{pmatrix} \tag{23}$$

The points of x are centered relatively to μ. It comes the two matrices

- D : matrix whose diagonal values are the eigenvalues of $\mathcal{C}$

$$D = \begin{pmatrix} 2{,}610^{-6} & 0 & 0 & 0 \\ 0 & 6{,}310^{-6} & 0 & 0 \\ 0 & 0 & 1{,}710^{-4} & 0 \\ 0 & 0 & 0 & 6{,}110^{-3} \end{pmatrix} \tag{24}$$

- E : matrix whose columns are the eigenvectors of $\mathcal{C}$

$$E = (\overrightarrow{v_1}, \overrightarrow{v_2}, \overrightarrow{v_3}, \overrightarrow{v_4}) = \begin{pmatrix} -0.1619 & -0.3393 & 0.7673 & 0.5196 \\ 0.3354 & -0.5046 & -0.5449 & 0.5796 \\ -0.7269 & 0.3911 & -0.3030 & 0.4763 \\ 0.5770 & 0.6909 & 0.1503 & 0.4089 \end{pmatrix} \tag{25}$$

In Figure 7 and 8, only the three eigenvectors $\overrightarrow{v_1}$, $\overrightarrow{v_2}$ and $\overrightarrow{v_3}$ are displayed.

And, then, the obtained whitening matrix U expressed in (8) based on D and E

$$U = \begin{pmatrix} -100.56 & 208.38 & -451.68 & 358.48 \\ -135.20 & -201.11 & 155.86 & 275.35 \\ 58.75 & -41.72 & -23.20 & 11.50 \\ 6.65 & 7.42 & 6.10 & 5.23 \end{pmatrix} \tag{26}$$

Therefore, the whitened mixtures V is the projection of X into U, as shown in equation (9). These resulting mixtures V are more appropriate for the source separation than the original mixtures X. Indeed, the sample v composed of the points belonging to V, shown in Figure 8, has the following appealing characteristics

- the zero arithmetic mean:

$$\mu = (0\ 0\ 0\ 0)^T \tag{27}$$

- the identity covariance matrix

$$\mathcal{C}' = \begin{pmatrix} 1 & 0 & 0 & 0 \\ 0 & 1 & 0 & 0 \\ 0 & 0 & 1 & 0 \\ 0 & 0 & 0 & 1 \end{pmatrix} \tag{28}$$

- the orthonormal basis composed by the eigenvectors corresponding to the columns of E.

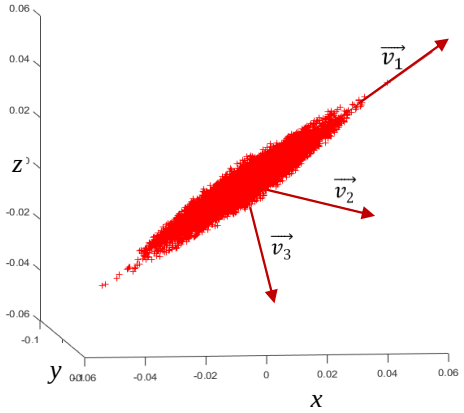

Fig. 7. Dispersity of points from mixtures before Whitening.

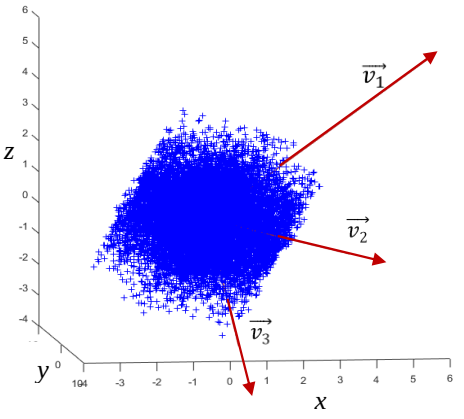

Fig. 8. Dispersity of points from mixtures after Whitening

D. Study of the source separation processing

In this section, the performance of the Fast–ICA algorithm is evaluated for the source separation task.

1) Performance measures

In the context of the separation of vibratory signal sources, performance measurement is an essential task for assessing separation quality. Therefore, the following measures are adopted [30]

- the Signal-to-Distortion Ratio (*SDR*)

$$SDR = 10\log_{10}\left(\frac{\left\|S_j^{target}\right\|^2}{\left\|e_j^{inter} + e_j^{artif}\right\|^2}\right) \quad (29)$$

- source-to-Interference Ratio (*SIR*)

$$SIR = 10\log_{10}\left(\frac{\left\|S_j^{target}\right\|^2}{\left\|e_j^{inter}\right\|^2}\right) \quad (30)$$

- the Souce-to-Artifact Ratio (*SAR*)

$$SAR = 10\log_{10}\left(\frac{\left\|S_j^{target} + e_j^{interf}\right\|^2}{\left\|e_j^{artif}\right\|^2}\right) \quad (31)$$

where

- $S_j^{target} = f(S_j)$ is a version of the original source modified using an allowed distortion $f \in F$, such that F encompasses several time-invariant gains distortions,
- e_j^{interf} and e_j^{artif} are, respectively, the error terms relative to interferences and artifacts.

2) Results and discussion

Our goal in this section is to identify the non-linearity results in the best performance of source separation using Fast–ICA algorithm. Furthermore, the experiments are conducted with healthy and faulty gears.

In the case of healthy mode, the results of table II are obtained. It is obvious that the tanh outperforms the other non-linearities. Indeed, it gives rise to the highest average values of *SIR*: 69.3 and *SDR*: 41.47.

Kurtosis gives the second best performance in terms of *SIR*: 65.87 and *SDR*: 38.02. The gauss non-linearity gives significantly lower average values of *SIR*: 27.23 and *SDR*: 21.95.

The worse performance is obtained by Skew non-linearity. It gives very low average value of *SIR*: 3.96 and *SDR*: 3.97. All the non-linearities result in close high *SAR* values between 41 and 44. Therefore, Fast–ICA leads to low overlap artifact in the estimated sources. In the case of faulty mixtures, the results of table III are obtained. Particularly, Fast–ICA performs the best separation using tanh non-linearity. It results in *SIR* average value 81.27 and *SDR* average value 48.15.

What is interesting in this faulty mode is that the sources of the damaged gear wheels R1 and R2 have been well separated based on tanh. Indeed, tanh gives rise the highest values of *SIR*: 88.67 and *SDR*: 59 for the estimated source of damaged wheel R1. Similarly, tanh gives the highest values of *SIR*: 75.75 and *SDR*: 38.85 for the estimated source of damaged wheel R2.

Moreover, the obtained average *SAR* values are between 45 and 48 for all the non-linearities. These values are higher than average *SAR* values obtained in the case of healthy mode. Therefore, Fast–ICA results in less overlap artifact in the faulty mode.

TABLE II. PERFORMANCE MEASURE OF SOURCE SEPARATION IN HEALTHY MODE

		Tanh	Kurtosis	Gauss	Skew
Nb of iterations		5	5	7	15
SIR (dB)	R1	70.4	70,1	60.8	5.7
	R2	64.3	61,4	3.86	1.98
	R3	65.9	62	40.4	2.4
	R4	76.6	70	3.86	5.77
	Average	69.3	65.87	27.23	3.96
SDR (dB)	R1	37.69	35.8	44.3	5.7
	R2	45	42.23	3.8	1.98
	R3	38.8	40.39	35.9	2.44
	R4	44.4	33.69	3.8	5.77
	Average	41.47	38.02	21.95	3.97
SAR (dB)	R1	37.69	38.8	44.4	47.63
	R2	45	45.26	56.6	40.19
	R3	38.8	44.41	37.7	36.34
	R4	44.4	37.69	37.9	46.86
	Average	41.47	41.54	44.15	42.75

TABLE III. PERFORMANCE MEASURE OF SOURCE SEPARATION IN FAULT MODE

		Tanh	Kurtosis	Gauss	Skew
Nb of iterations		5	5	7	15
SIR (dB)	R1	88.67	71.94	84.7	2.39
	R2	75.75	72.01	71.5	-4.1
	R3	73	71.07	70.3	1.3
	R4	87.67	86.5	66.4	3.5
	Average	81.27	75.38	73.22	0.77
SDR (dB)	R1	59	37.68	55	2.39
	R2	38.85	36.7	37.7	-4.13
	R3	37	38.8	38.8	1.37
	R4	57.75	59	37.68	3.5
	Average	48.15	43.04	42.29	0.78
SAR (dB)	R1	59	37.68	59	41.54
	R2	38.85	57.75	57.7	37.89
	R3	37.68	38.85	38.8	61.29
	R4	57.75	59	37.6	41.6
	Average	48.32	48.32	48.27	45.58

IV. SPECTRAL ANALYSIS

In this section, the results obtained by the Fast–ICA algorithm are studied. First, Fast–ICA converges quickly in up to 15 iterations, which confirms that this algorithm is a fast variant of the ICA. On the other hand, in our experiments, Fast–ICA is applied on two types of mixing: healthy mode and fault mode. Therefore, two questions that arise: Is the Fast–ICA able to separate the gear signals associated to the four

wheels R1, R2, R3 and R4? And, in the case of a fault mode, can it distinguish between damaged wheels and healthy wheels ?

By observing the spectrums of the estimated sources, Fast–ICA succeeded in separating the gear signals corresponding to each wheel. The spectrum presented in Figure 9 is composed of a fundamental frequency $f_{mesh,12}$ and two lateral frequencies $f_{l,1}$ and $f_{r,1}$. Thus, the source 1 corresponds to the wheel R1. The second spectrum illustrated in Figure 10 is composed of a fundamental frequency $f_{mesh,12}$ and two lateral frequencies $f_{l,2}$ and $f_{r,2}$. Thus, the source 2 identifies the wheel R2. The third spectrum shown in Figure 11 is composed of a fundamental frequency $f_{mesh,34}$ and two lateral frequencies $f_{l,3}$ and $f_{r,3}$, leading to a clear identification of wheel R3. Finally, the spectrum given in Figure 12 is composed of a fundamental frequency $f_{mesh,34}$ and two lateral frequencies $f_{l,4}$ and $f_{r,4}$. Thus, the source 4, corresponding to the wheel R4, is clearly identified.

By comparing the results obtained in fault mode with the results obtained in healthy mode, Fast–ICA distinguishes between the faulty sources and the healthy sources of the gears

- The wheel R1 has two slightly different spectrums. Indeed, the spectrum of the wheel R1 mentioned in Figure 13 is slightly different from the spectrum of R1 in Figure 9 which is in a healthy mode.
- The wheel R2 has two slightly different spectrums. Indeed, the spectrum of the wheel R2 mentioned in Figure 14 is slightly different from the spectrum of R2 in Figure 10 which is in a healthy mode.
- On the other hand, the other two wheels R3 and R4 are healthy. Indeed, each of these two wheels keeps almost the same spectrum in the healthy mode and in the fault mode, as shown in Figures (15, 11) and Figures (16, 12) respectively.

V. CONCLUSION

In this paper, a diagnostic technique is presented for separating and identifying uniform wear in two-stage gearbox, classically associated to a double-fed induction machine in modern wind energy conversion systems. Based on Fast–ICA, the main contribution of the proposed technique is its ability to isolate the fault frequency components, representative of a uniform wear for each pinion or gear of the gearbox.

The obtained results show also clearly the ability of the Fast–ICA for separating the characteristic frequency components of the gears from noisy mixtures. Moreover, the spectral analysis allows us to distinguish for each estimated source associated to a gear whether it is healthy or faulty. As a perspective, further faults than gear fault would be taken into account in a future work.

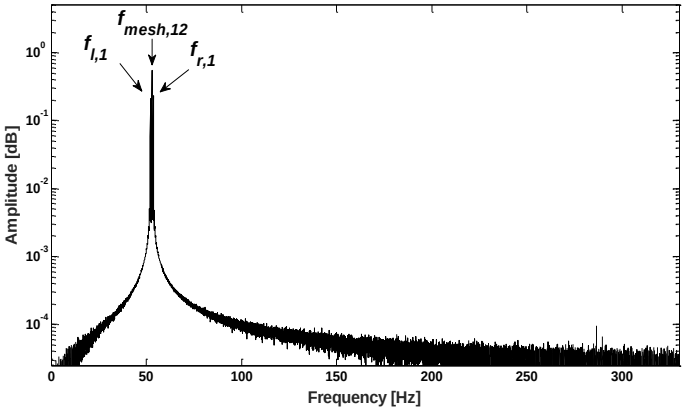

Fig. 9. Spectrum of signal resulting from the estimation of component relative to the wheel R1, in healthy mode.

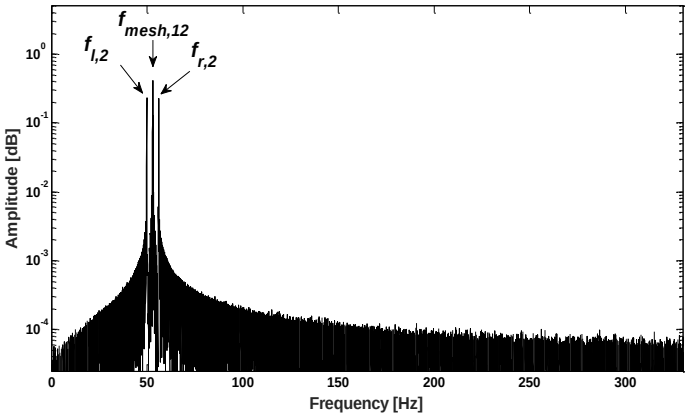

Fig. 10. Spectrum of signal resulting from the estimation of component relative to the wheel R2 in healthy mode.

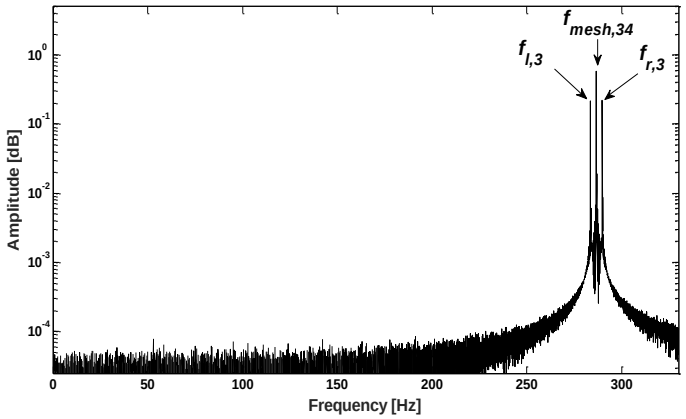

Fig. 11. Spectrum of signal resulting from the estimation of component relative to the wheel R3, in healthy mode.

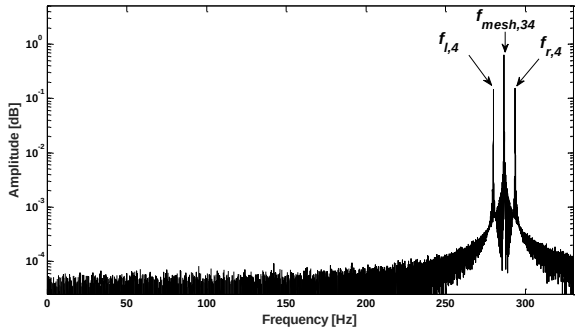

Fig. 12. Spectrum of signal resulting from the estimation of component relative to the wheel R4, in healthy mode.

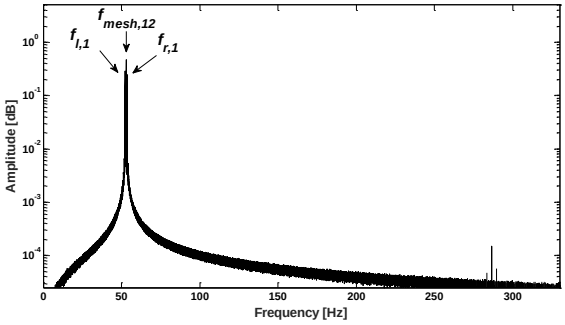

Fig. 13. Spectrum of signal resulting from the estimation of component relative to the wheel R1, in fault mode with uniform wear of R1 and R2.

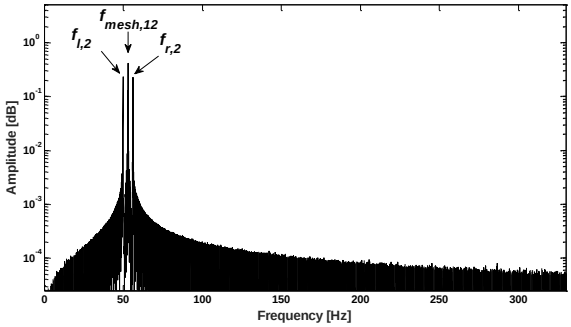

Fig. 14. Spectrum of signal resulting from the estimation of component

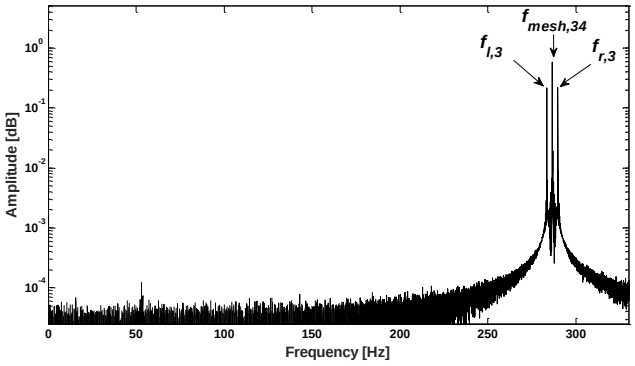

Fig. 15. relative to the wheel R2, in fault mode with uniform wear of R1 and R2.

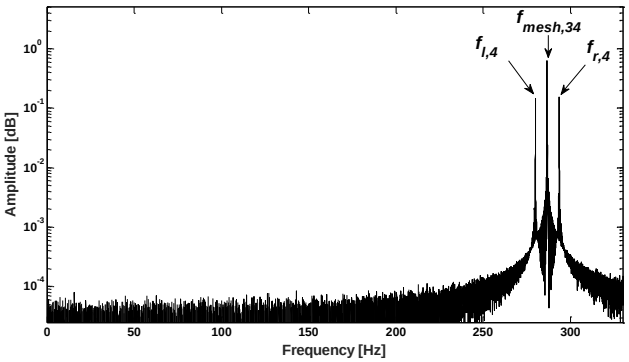

Fig.

Fig. 16. Spectrum of signal resulting from the estimation of component relative to the wheel R4, in fault mode with uniform wear of R1 and R2.

REFERENCES

[1] H. Polinder, F.A. Van Der Pijl, G-J. de Vilder and P.J. Tavner, "Comparison of Direct-Drive and Geared Generator Concepts for Wind Turbines", IEEE Transactions on Energy Conversion, vol. 21, no. 3, Sept. 2006, pp. 725-733.

[2] H. Li, Z. Chen, "Design optimization and evaluation of different wind generator systems", The 2008 International Conference on Electrical Machines and Systems, 17-20 Oct. 2008, pp. 2396 – 2401.

[3] Y. Amirat, M.E.H. Benbouzid, E. Al-Ahmar, B. Bensaker, S. Turri, "A brief status on condition monitoring and fault diagnosis in wind energy conversion systems", Renewable and Sustainable Energy Reviews, vol. 13, no. 9, Dec. 2009, pp. 2629–2636.

[4] M. Todorov, I. Dobrev, and F. Massouh, "Analysis of Torsional Oscillation of the Drive Train in Horizontal-Axis Wind Turbine", Electromotion 2009 – EPE Chapter 'Electric Drives' Joint Symposium, Lille, 1-3 July 2009.

[5] N. Baydar, A. Ball, "Detection of gear failures via vibration and acoustic signals using wavelet transform", Mechanical Systems and Signal Processing, vol. 17, no. 4, pp. 787-804, 2003.

[6] S. Slim, Van L. Paul, P. Asanka, Gan Tat-Hean, B. Bryan", Determination of the combined vibrational and acoustic emission signature of a wind turbine gearbox and generator shaft in service as a pre-requisite for effective condition monitoring", Renewable Energy, vol. 51, 2013, pp. 175–81.

[7] M. Heydarzadeh, M. Nourani, J. Hansen and S.H. Kia, "Non-invasive gearbox fault diagnosis using scattering transform of accoustic emission", IEEE-ICASSP, New Orleans, pp. 371-375, March 2017.

[8] J. Wei and J. McCarty, "Acoustic emission evaluation of composite wind turbine blades during fatigue testing", Wind Eng., vol. 17, no. 6, pp. 266-274, 1993.

[9] D. Coronado, C. Kupferschmidt, "Assessment and validation of oil sensor systems for on-line oil condition monitoring of wind turbine gearboxes", 2nd International Conference on System-Integrated Intelligence: Challenges for Product and Production Engineering, vol. 15, pp 748 –755, 2014.

[10] D. Dyer, R.M. Stewart, "Detection of rolling element bearing damage by statistical vibration analysis", Trans ASME, J Mech Design, vol. 100, no. 2, pp. 229–235, 1978.

[11] N.J. Cozens, S.J. Watson, "State of the art condition monitoring techniques suitable for wind turbines and wind farm applications", Report for CONMOW, Project 2003.

[12] Y. Gritli, A. Di Tommaso, R. Miceli, C. Rossi and F. Filippetti, "Diagnosis of mechanical unbalance for double cage induction motor load in time-varying conditions based on motor vibration signature analysis", International Conference on Renewable Energy Research and Applications,Madrid, pp. 1157-1162, 2013.

[13] R. Miceli, Y. Gritli, A. Di Tommaso, F. Filippetti and C. Rossi, "Vibration signature analysis for monitoring rotor broken bar in double squirrel cage induction motors based on wavelet analysis", The

International Journal for Computation and Mathematics in Electrical and Electronic Engineering, vol. 33, pp. 1625-1641, 2014.

[14] V. Capdevielle, C. Serviere and J.L. Lacoume, "Blind separation of wide- band sources: Application to rotating machine signals", 8th European Signal Processing Conference, Triest, September, 1996.

[15] T.D. Popescu, "Blind separation of vibration signals and source change detection – Application to machine monitoring", Applied Mathematical Modelling, vol. 34, pp. 3408-3421, 2010.

[16] A. Hyvärinen and E. Oja, "Independent component analysis: algorithms and applications", Neural networks, vol. 13, pp. 411–430, 2000.

[17] F. Miao and R. Zhao, "Application of Independent Component Analysis in machine fault diagnosis", Advanced Materials Research, vol. 905, pp. 524-527, 2014.

[18] Z. Xing yuan, T. Ji Liang, and D. De cun, "Separation of the Train Vibration Signal Based on Improved Fast-ICA", IEEE Computer Society, Fourth International Conference on Intelligent Computation Technology and Automation, Washington, Vol. 1, pp. 912-914, 2011.

[19] H. Nakamura and al., "The application of independent component analysis to the multi-channel surface electromyographic signals for separation of motor unit action potential trains: part I – measuring techniques", J. Electromyogr Kinesiol, vol. 14, pp. 423-432, 2004.

[20] D. Obradovic, N. Madhu, A. Szabo, C.S. Wong, "Independent component analysis for semi-blind signal separation in MIMO mobile frequency selective communication channels", IEEE International Joint Conference on Neural Networks,Munich, pp. 53–58, 2004.

[21] A. Ypma, A. Leshem, and R.P. Duin, "Blind separation of rotating machine sources: bilinear forms and convolutive mixtures", Neurocomputing, vol. 49, pp. 349–368, 2002.

[22] G. Yu, "Fault feature extraction using independent component analysis with reference and its application on fault diagnosis of rotating machinery", Neural Computing and Applications, vol. 26, pp. 187-198, 2015.

[23] A-J. Bell, T-J. Sejnowski, "An information maximization approach to blind separation and blind deconvolution", Neural Comput., vol. 7, pp. 1129–1159, June 1995.

[24] J.F. Cardoso, A. Souloumiac, "Blind beamforming for non gaussian signals", in IEE Proceedings-F., vol. 140, no. 6, pp. 362–370, Dec. 1993.

[25] J. Zhang, A. C. Sanderson, "JADE: Self Adaptive Differential Evolution with fast and reliable convergence performance", IEEE Congress on Evolutionary Computation,Troy, vol. 13, no 5, pp. 945-958, 2009.

[26] A. Hyvarinen and E. Oja, "A fast fixed-point algorithm for independent component analysis", Neural Computition, vol. 9, pp. 1483–1492, 1997.

[27] A. Hyvarinen, J. Karhunen and E. Ojaa, "Independent Component Analysis", Hoboken, NJ: Wiley-Interscience, 2001.

[28] M. Farhat, Y. Gritli, M. Benrejeb, "Application de l'analyse en composantes indépendantes pour l'identification de défauts mécaniques d'une chaîne de conversion éolienne", ICME International Conference on Mechatronics Engineering, Sousse, 2017.

[29] A. Hyvärinen, "Fast and Robust Fixed-Point Algorithms for Independent Component Analysis", IEEE Trans. on Neural Networks, vol. 10, no. 3 pp. 626-634, mai 1999.

[30] E. Vincent, R. Gribonval and C. Févotte, "Performance measurement in blind audio source separation", IEEE Transactions on Audio, Speech and Language Processing, vol. 14, no. 4, pp. 1462–1469, July 2006.